THE SPECIFICATION OF RADIATIVELY CONSTRAINED, EFFECTIVE CLOUDS IN GCM's: METHODOLOGY AND SOME PRELIMINARY RESULTS

Charles Tony Gordon
Geophysical Fluid Dynamics Laboratory
Princeton New Jersey

ABSTRACT

We formulate an algorithm (SATCLD) to generate fields of radiatively constrained effective cloud amount for general circulation models (GCM's) from compact, accessible analyses of satellite-derived radiative flux data. Then the plausibility of some effective cloud fields generated by SATCLD is discussed. The work of Gordon (1983) has been extended in three ways. First, some new sensitivity experiments have been performed, which indicate a favorable response to an improved specification of surface albedo and improved analysis of satellite-derived radiative flux data. Second, effective cloud amount fields, which have been generated for the period 10-14 June 1979, simulate the sudden onset of the summer Indian monsoon. Third, a radiatively-constrained critical relative humidity scheme for predicting cloud amount in GCM's has recently been developed.

1. INTRODUCTION

The radiative treatment of clouds affects the horizontal and vertical distributions of model-predicted radiative flux, which in turn may affect the atmospheric circulation, viz. radiative-dynamic coupling, as noted by Stephens and Webster, (1981), Ramanathan et al., (1983) and others. Hence, this subject is of practical concern to modellers engaged in GCM climate sensitivity or long range weather prediction experiments.

An important class of cloud parameters of present generation GCM's

is "cloud amount," which will refer collectively to the respective fractions of a grid box containing low, middle, and/or high cloud. Typically, cloud amount is specified from climatology or observation, or is parameterized in terms of model-predicted thermodynamic variables.

The effect of cloud amount upon the distribution of model-predicted radiative flux is of ultimate interest. However, we shall restrict our attention here to "model-diagnosed" radiative fluxes. By definition, such fluxes are calculated by a GCM's cloud-radiation model from observed (as opposed to model-predicted) temperature and water vapor fields, and specified cloud amount fields. Intuitively, a fairly high degree of consistency between model-diagnosed versus observed longwave, shortwave and net radiative fluxes should be one of the prerequisites for generating reasonable model-predicted radiative flux fields. But judging from the results of Gordon, et al., (1984), (hereafter referred to as GHS), radiative consistency is rather elusive if currently available observed cloud amount fields are specified.

Among the factors which contribute to radiative inconsistency are deficiencies in: (1) the observed cloud amount data set itself; (2) the GCM's cloud-radiation model, e.g., parameterizations of cloud top height, emissivity, cloud albedo, etc.; (3) the GCM's surface albedo field, especially over deserts and snow/ice surfaces; and (4) analyses of temperature, water vapor and/or radiative flux observations. Thus, radiative inconsistency would be likely to occur even if the (externally produced) fields of observed cloud amount were perfect.

Under these circumstances, modellers could adapt their GCM's to be compatible with the models used to generate future, more accurate cloud data sets and those used to convert raw radiance data to analyses of

broad band radiative flux. But an alternative interim strategy, (the one proposed here) is to generate "effective" clouds for one's own GCM. By definition, "effective" clouds are constrained to be consistent with observed longwave as well as shortwave radiative fluxes, and they are GCM-dependent. Hence, they inherently compensate for biases in the cloud-radiation model, surface albedo field, etc. of the GCM in question, as well as incorporate biases of observed satellite-derived radiative fluxes and other input data.

There are potentially two advantages of specifying effective clouds in GCM's. First, they would constrain GCM-diagnosed radiative fluxes to be more or less consistent with observation. This could be beneficial, provided that deficiencies in the analyses of the observed satellite data were not the dominant contributing factor to radiative inconsistencies. Second, a comparison of effective clouds and corresponding GCM-diagnosed radiative fluxes with observation would afford modellers the opportunity to become more aware of radiation-related biases in their GCM's as well as in analyses of observed satellite data, and perhaps motivate them to improve the treatment of radiative transfer, clouds, aerosols and/or surface albedo in their GCM's. Through an iterative process, effective cloud fields could become more realistic.

In keeping with the spirit of the SATCLD approach, we have employed a typical GCM, i.e., the Geophysical Fluid Dynamics Laboratory (GFDL) spectral extended range prediction model and convenient satellite-derived radiative flux data sets despite limitations of both. We note that there are not enough degrees of freedom in the archived radiative flux data, currently available, to capture all of the impor-

tant properties which characterize real clouds or to independently validate the SATCLD effective clouds.

Schneider (1972) used the concept of effective clouds to discuss the sensitivity of global mean climate to global mean cloudiness. His variables were global mean effective cloud top height and cloud cover fraction of a single layer of clouds. However, for GCM applications, the desired effective cloud top height will not necessarily coincide with any of the fixed vertical levels of the GCM in question. The resulting discrepancy could be potentially rather substantial if the spacing between adjacent levels were to exceed 50 to 75 mb in the upper troposphere. In contrast, effective cloud amounts for two distinct cloud layers can be finely tuned to attain radiative consistency, locally. Therefore, we have modified Schneider's approach such that the variables are grid point values of effective low and high cloud amount, while the cloud tops and bases are fixed a priori. Global analyses of effective low or high cloud amount can be built up from solutions at each GCM grid point.

Another key feature of the SATCLD scheme is that it utilizes compact, readily available data sets of analyzed long- and shortwave radiative fluxes. The tape volume of archived data requiring processing is relatively minimal, by virtue of its 250-500 km, GCM-compatible spatial resolution. This may be quite advantageous, since it would be unfeasible for most modellers to work directly with pixel scale radiance data. Moreover, the scheme is economical to apply, at least for two (or three) cloud parameters.

2. DESCRIPTION OF THE SATCLD SCHEME

The GCM-dependent fields of effective low and high cloud amount

will hereafter be referred to as SATCLD clouds and the algorithm for computing them as SATCLD. The first step is to expand the observed, satellite-derived absorbed shortwave radiative flux, S_{OBS} and outgoing longwave flux, F_{OBS} as second order Taylor series in the unknown cloud amount variables. More precisely, at each grid point of our spectral GCM:

$$S_{OBS} = S_o + \left(\frac{\partial S}{\partial n_h}\right)_o \Delta n_h + \left(\frac{\partial S}{\partial n_l}\right)_o \Delta n_l + \frac{1}{2}\left(\frac{\partial^2 S}{\partial n_h^2}\right)_o \Delta n_h^2 + \frac{1}{2}\left(\frac{\partial^2 S}{\partial n_l^2}\right)_o \Delta n_l^2 + \left(\frac{\partial^2 S}{\partial n_h \partial n_l}\right)_o \Delta n_h \Delta n_l + \varepsilon_S \qquad (1)$$

$$F_{OBS} = F_o + \left(\frac{\partial F}{\partial n_h}\right)_o \Delta n_h + \left(\frac{\partial F}{\partial n_l}\right)_o \Delta n_l + \frac{1}{2}\left(\frac{\partial^2 F}{\partial n_h^2}\right)_o \Delta n_h^2 + \frac{1}{2}\left(\frac{\partial^2 F}{\partial n_l^2}\right)_o \Delta n_l^2 + \left(\frac{\partial^2 F}{\partial n_h \partial n_l}\right)_o \Delta n_h \Delta n_l + \varepsilon_F \qquad (2)$$

In the above equations, n_h and n_l are the effective fractional high and low cloud amounts. Also, S and F are model-diagnosed short- and longwave radiative fluxes, i.e., they are computed by the GCM's cloud-radiation model from observed meteorological data. The "o" subscript indicates that the model-diagnosed fluxes or derivatives correspond to known reference values of high cloud amount n_{h_o} and low cloud amount n_{l_o}. The unknowns Δn_h and Δn_l represent the departures $n_h - n_{h_o}$ and $n_l - n_{l_o}$, while ε_S and ε_F are residuals.

The standard observed fluxes S_{OBS} and F_{OBS} were obtained from the

National Environmental Satellite Data Information Service (NESDIS) 2.5° x 2.5° archive of earth radiation budget data for January 1977 (NOAA-5) and July 1979 (TIROS N) and interpolated to the 3.3° x 5.6° latitude-longitude grid of our GCM. This data was chosen for its availability and compactness as well as our need to keep the data processing to manageable proportions.

The desired solution at a particular grid point is the pair of fractional cloud amounts n_l and n_h which minimizes the sum of the squares of the residuals in the Taylor series expansions for S_{OBS} and F_{OBS}. Mathematically, the minimization criterion may be expressed as

$$\left(\varepsilon_s^2 + \varepsilon_F^2\right)\{n_h, n_l\} = \text{minimum} \qquad (3)$$

Also, when necessary, two constraints are invoked to guarantee physical realizability:

$$0 \leq n_h \leq 1 \qquad (4a)$$

$$0 \leq n_l \leq 1 \qquad (4b)$$

Equation (3) constrains the cloud amounts n_l and n_h to be consistent with the observed net radiative flux $R_{OBS} = S_{OBS} - F_{OBS}$, provided equations (4a) and (4b) are not invoked. Thus, the squared residual net flux $(\varepsilon_s - \varepsilon_F)^2$ will usually be small, even if not rigorously minimized. Moreover, Eq. (3) will tend to exclude solutions whose residuals ε_S and ε_F are individually large but fortuitously cancel.

An approximate solution is readily obtained by trial and error, through varying n_l and n_h independently in increments of 0.01. The partial derivatives in Equations (1) and (2) are computed, a priori, using centered fininte difference approximations. For this purpose, S and F

are diagnosed by the GCM's cloud-radiation model for various combinations of n_l and n_h, and the same monthly mean (or instantaneous) analyses of observed temperature and water vapor. In practice, the contribution of the second derivative terms tends to be negligible.

The spectral GCM, has been discussed by GHS. It is rhomboidally truncated at wavenumber 21, has 9 vertical levels, employs the so-called E4 parameterization of sub-grid scale vertical mixing, and is referred to as R21L09 E4. An R30L09 E4 version has been described in even greater detail by Gordon and Stern (1982). The Fels-Schwarzkopf (1975) radiation model is an important component of the GCM. The cloud top heights and bases are the same as in GHS. They are functions of latitude and season, after Telegadas and London (1954). The fixed cloud absorptivities and zenith angle-dependent cloud albedo formulae correspond, respectively, to the January 1977 standard absorptivities and optional albedos of GHS. The standard surface albedo field is based upon the Posey and Clapp (1964) analysis over land, and the Payne (1972) formulation over the open oceans. The standard surface albedo of sea ice is fixed, while that of snow equals 0.75 within the polar cap and varies only with snow depth elsewhere. The snow depth is from an Air Force Global Weather Central (AFGWC) analysis over the northern hemisphere in winter and GCM climatology elsewhere.

The standard meteorological analyses of atmospheric variables, e.g. temperature, for January 1977 and July 1979 were essentially monthly means of the NMC analyses for those months. The only exception was H_2O mixing ratio, which was obtained from an optimal interpolation analysis of dew point depression station data.

3. COMPARISON OF SATCLD, 3DNEPH AND SFCOBS CLOUDS

Monthly mean analyses of SATCLD effective low and high cloud amount have been compared with: (i) 3DNEPH - A northern hemispheric analysis of low, middle and high cloud amount compressed from the voluminous global AFGWC 3D-Neph analysis, which is based primarily upon NOAA-5 and DMSP satellite observations in January 1977 and July 1979, respectively; (ii) SFCOBS - An objective analysis of low, middle and high cloud amount which is based exclusively upon surface observations of clouds. The 3DNEPH and SFCOBS analyses are described more extensively in GHS.

A quantitative verification is not possible because: (1) the "ground truth" is not known; (2) there is a discrepancy in the implied definitions of cloud amount as seen by satellite vs. from the ground; (3) there are two levels of effective clouds vs. three levels of 3DNEPH and SFCOBS clouds; (4) the input data used to generate SATCLD, 3DNEPH and SFCOBS clouds are not spatially or temporally synchronized. Nonetheless, the plausibility of SATCLD clouds can be qualitatively assessed.

Monthly mean SATCLD and 3DNEPH cloud amount fields are illustrated for January 1977 (Figure 1) and July 1979 (Figure 2). The SATCLD analyses of high (n_h) and low (n_l) effective cloud amount seem plausible in the tropics and subtropics (excluding deserts), where the radiation budget at the top of the atmosphere is more sensitive to clouds than to surface albedo or surface temperature. For example, they contain dry zones over the subtropical oceans and well-defined ITCZ's as does the 3DNEPH. Second, the July 1979 SATCLD and 3DNEPH fields of high cloud amount, n_h, are in quite good agreement, in the tropics (and even in the summer northern hemisphere extratropics). Third, in the well-known

regions of stratocumulus formation off the west coasts of Peru and southern Africa, the SATCLD effective low cloud resembles SFCOBS (not shown) in July. On the other hand, there are some substantial differences in July between SATCLD and 3DNEPH, e.g. in the intensity of the ITCZ, "dry zones" over the subtropical oceans and convection over the southeastern United States. The latter two discrepancies may be related to the use of different satellites, i.e., TIROS N vs. DMSP, in July 1979. In particular, note that the TIROS N satellite crosses the equator during mid-afternoon (1500 GMT) local time, compared to the early morning/evening or noontime for the AFGWC's two DMSP satellites. At mid-latitudes, the SATCLD effective low cloud amount field bears only a vague resemblance to the 3DNEPH and/or SFCOBS, mainly over the oceans. Also, the SATCLD analysis is not very realistic over subtropical deserts (note the low clouds over the Sahara Desert) or over snow-covered mid-latitude terrain, due perhaps to biases in the GCM's standard specification of surface albedo. Moreover, hardly any SATCLD Arctic stratus is found, in part because the standard surface albedo over the permanent polar cap is excessive. The SATCLD low overcast between 40°S - 60°S (not shown) may be attributable to the neglect of bi-directional reflectance and zenith angle-dependence in the NESDIS analysis algorithms described in Gruber (1978). Within the polar night region, the SATCLD scheme is inherently ill-conditioned.

4. CHECK OF RADIATIVE CONSISTENCY

Model-diagnosed radiative fluxes at the top of the atmosphere for January 1977 and July 1979 have been compared with NOAA-5 and TIROS N satellite data, respectively, The calculations provided a self-consistency check of the SATCLD algorithm as well as some insights into

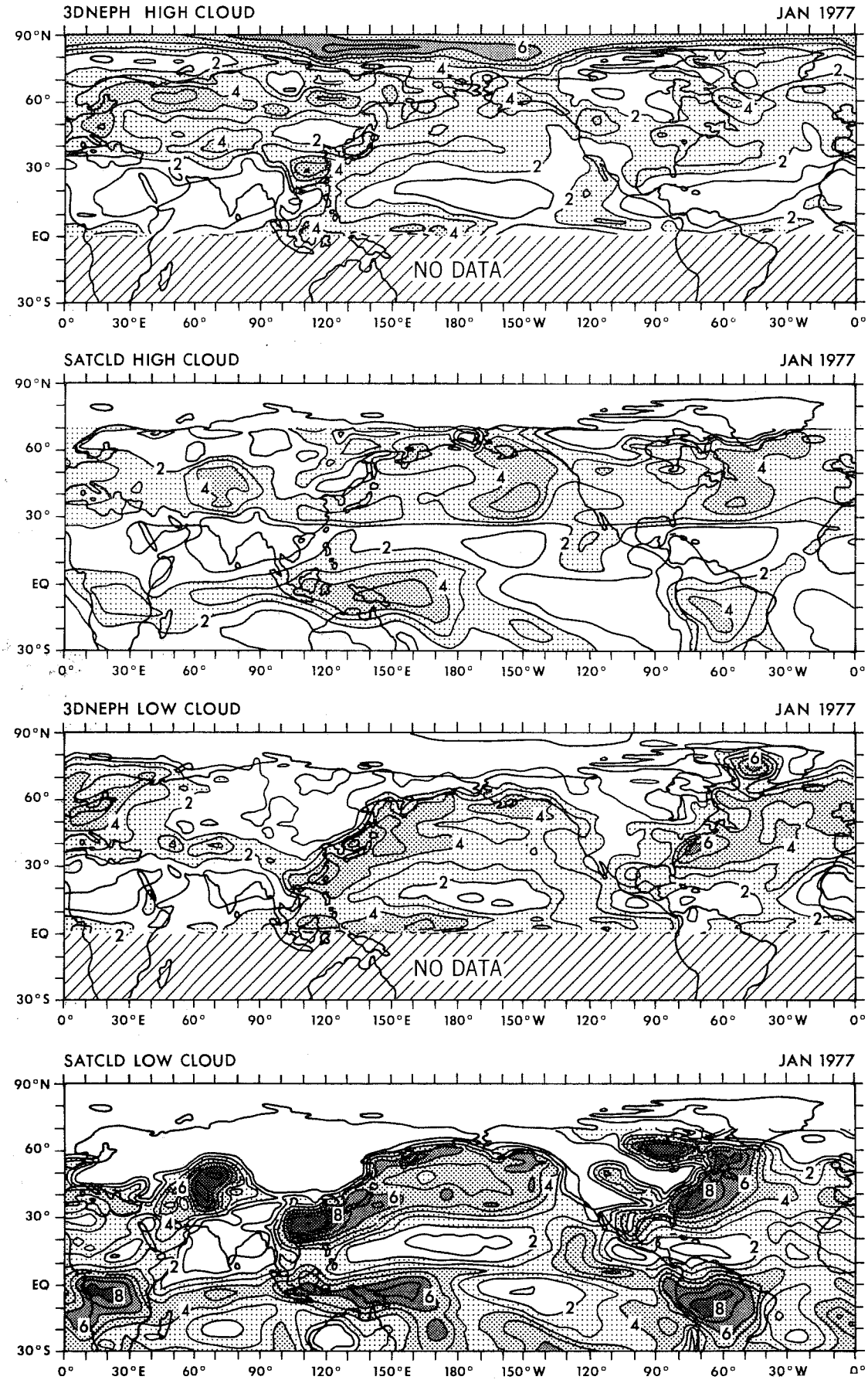

Fig. 1. Monthly mean low and high cloud amount for January 1977. Contour interval = 0.1. Stippling interval = 0.2.

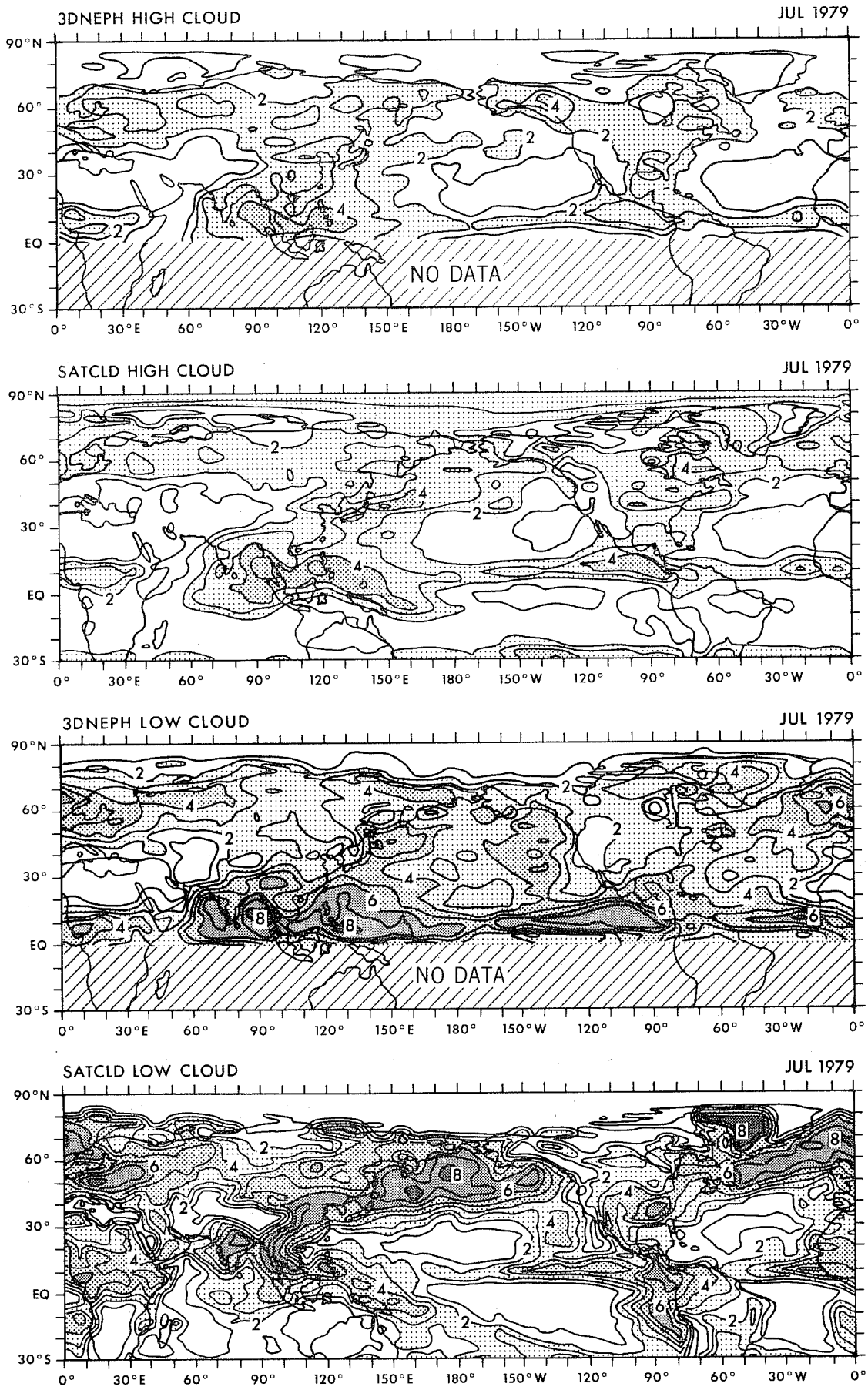

Fig. 2. Same as Fig. 1 except for July 1979.

possible causes of robust GCM-dependent and/or observation-dependent biases, i.e., biases which activate the physical realizability constraints (4a) and (4b).

5. NEW SENSITIVITY EXPERIMENTS

In the practical application of the SATCLD algorithm, the modeller would be confronted by uncertainties in the surface albedo field, observed state of the atmosphere and satellite-derived radiative flux data. Therefore, we have examined the sensitivity of our SATCLD effective cloud fields to: (i) new vs. standard surface albedo; (ii) new vs. standard analysis of observed atmospheric variables; and (iii) new vs. standard satellite-derived analysis of radiative fluxes. A second goal is to obtain more realistic effective cloud fields. The emphasis will be on map intercomparisons, since the spatial distribution of the discrepancies may be useful to the modeller.

5.1 Surface albedo

The new specification of surface albedo, A_s, is presumably more accurate. It utilizes CLIMAP surface albedos corresponding to dry, wet or (fresh, deep) snow-covered conditions for various land surface types, as well as model-diagnosed soil moisture, satellite-derived snow cover and a surface temperature-dependent parameterization of A_s over melting snow. The latter parameterization is similar to, but somewhat less extreme than that of Robock (1980). Its use caused A_s over snow-covered land and sea ice in the summer Arctic to decrease from 0.75 to ~0.55. The new and standard July surface albedo fields and the (new - standard) difference field are shown in Figure 3. Similarly, the corresponding new and standard n_1 fields are shown in Figure 4. With the new surface albedo field, SATCLD low effective cloud amount decreases slightly over

the southeastern United States, decreases over the Sahara Desert and increases over the permanent Arctic snow pack. Intuitively, these changes seem to be in the right direction.

5.2 Meteorological analysis

Next, SATCLD effective clouds have been computed for the July 1979 monthly means of two meteorological analyses of atmosphere temperature and water vapor: the "new" GFDL 4-dimensional FGGE analysis (Ploshay,et al, 1983) vs. the "standard" analysis. The standard (TIROS N) July 1979 monthly mean analyses of satellite-derived radiative fluxes and the new surface albedo field are specified.

The essential differences between the two meteorological analyses have yet to be analyzed. In any case, the differential high cloud amount Δn_h is generally < 0.1, except over parts of southern Canada and northeast Asia where $\Delta n_h \sim +0.2$. (In contrast, the seasonal variation of H_2O vapor yields a systematic extratropical response of 0.1 to 0.2.) The discrepancy for low cloud amount is generally small, except locally near the periphery of the Arctic sea ice margin. There, the model-calculated surface temperature and hence the surface albedo are sensitive, perhaps, to the boundary layer temperature and humidity fields.

5.3 Satellite-derived radiative flux

In a third experiment, only the satellite-derived radiative flux data has been varied. The standard and new data sets are respectively the TIROS N, and the narrow field of view NIMBUS 7 ERB matrix data (NASA; 1978). The NIMBUS 7 data were archived on an equal area grid having approximately 4.5° resolution. The new surface albedo field and the new (i.e., GFDL FGGE) analysis were specified.

The July 1979 monthly mean TIROS N and NIMBUS 7 absorbed short-

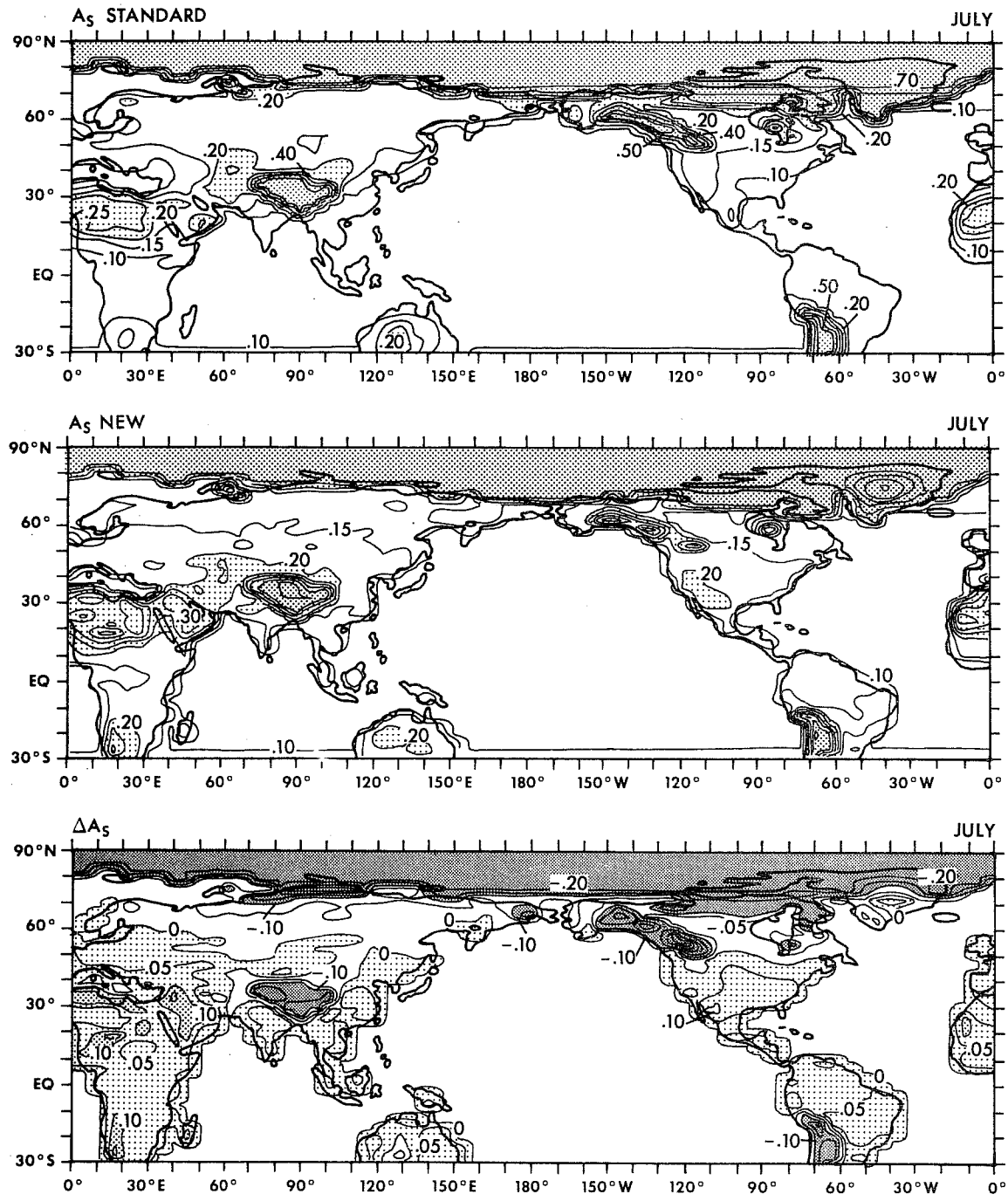

Fig. 3. July monthly mean surface albedo. Standard A_S (top), new A_S (middle), new-old differential albedo ΔA_S (bottom). Contour interval = 0.05 or 0.10 for A_S; 0.05 for ΔA_S.

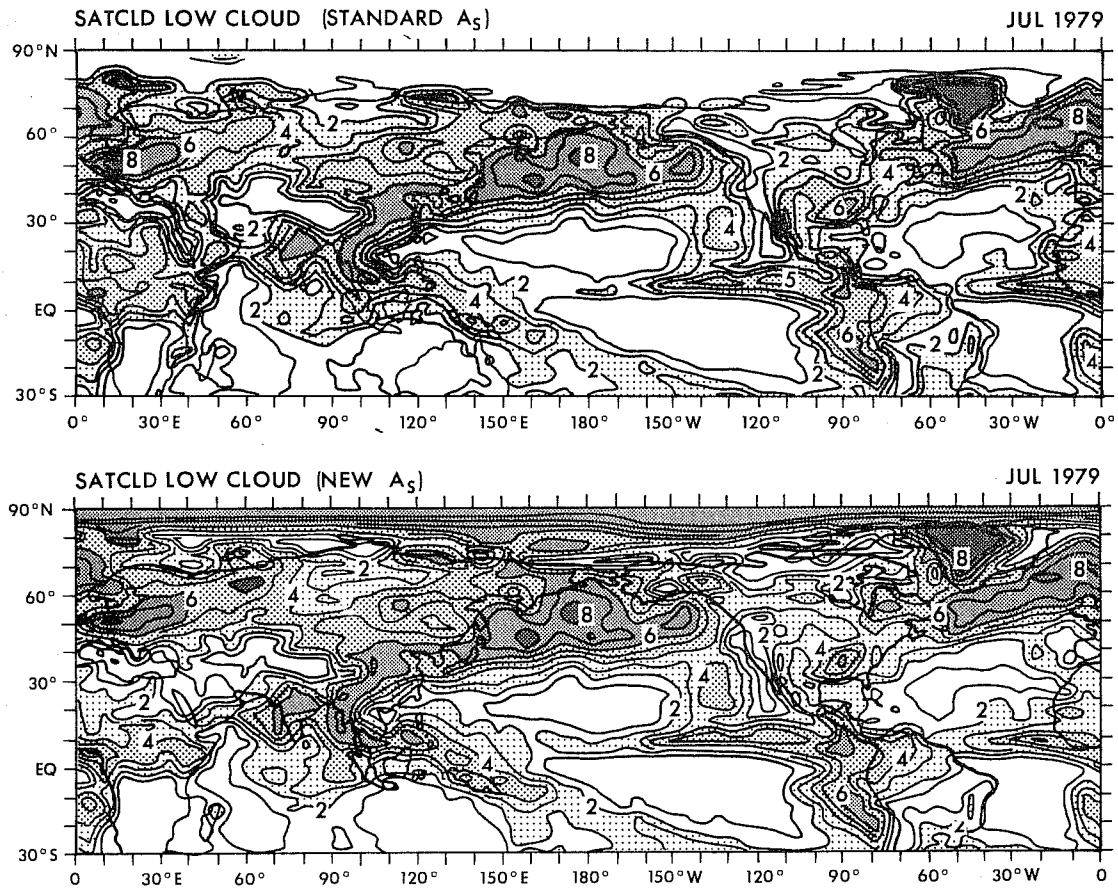

Fig. 4. July 1979 monthly mean SATCLD low cloud amount corresponding to the standard A_S (top) and new A_S (bottom). Contour interval and stippling as in Fig. 1.

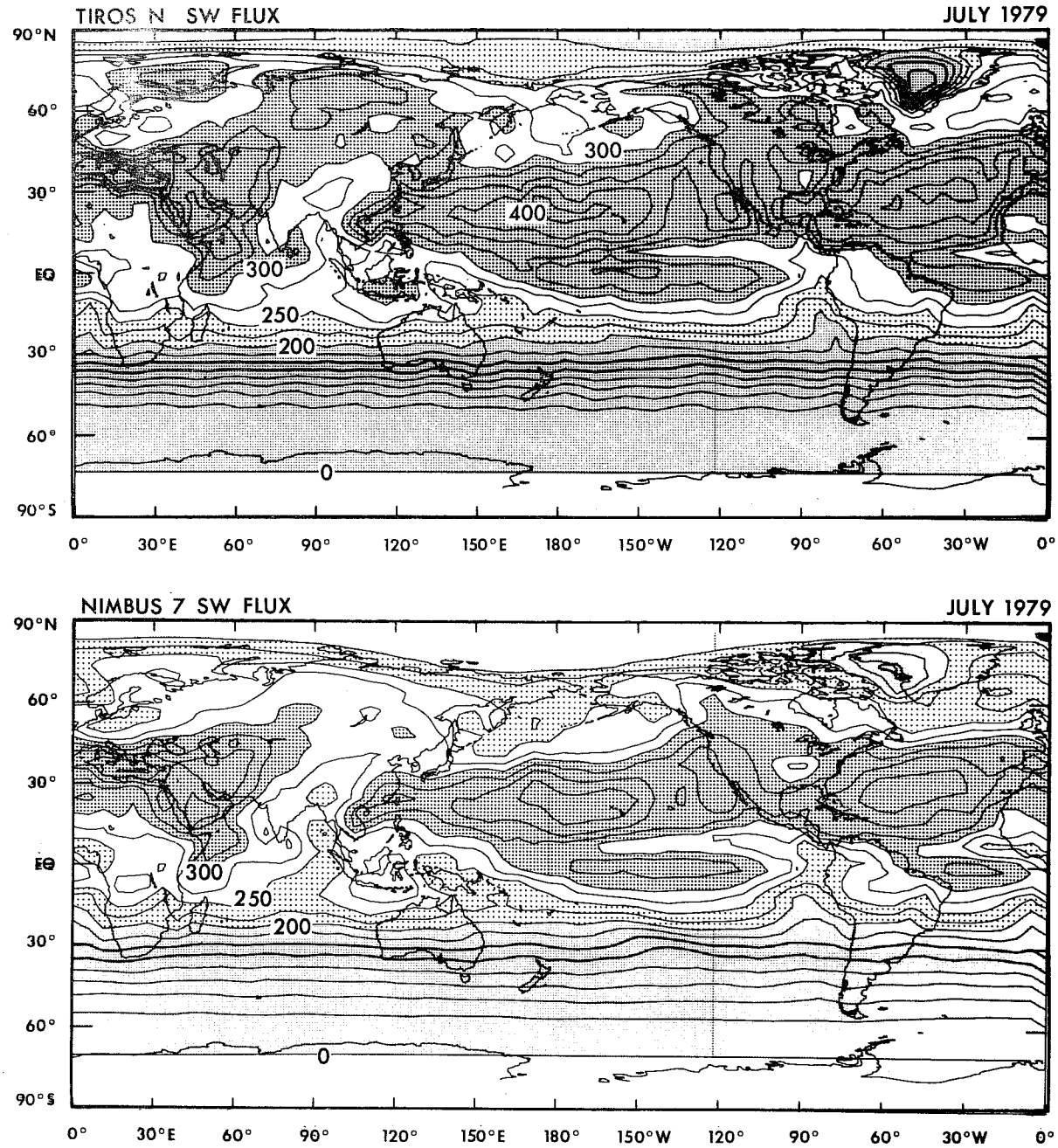

Fig. 5. July 1979 monthly mean net absorbed shortwave radiative flux, TIROS N (top) and NIMBUS 7 (bottom). Contour interval = 25 W m^{-2}.

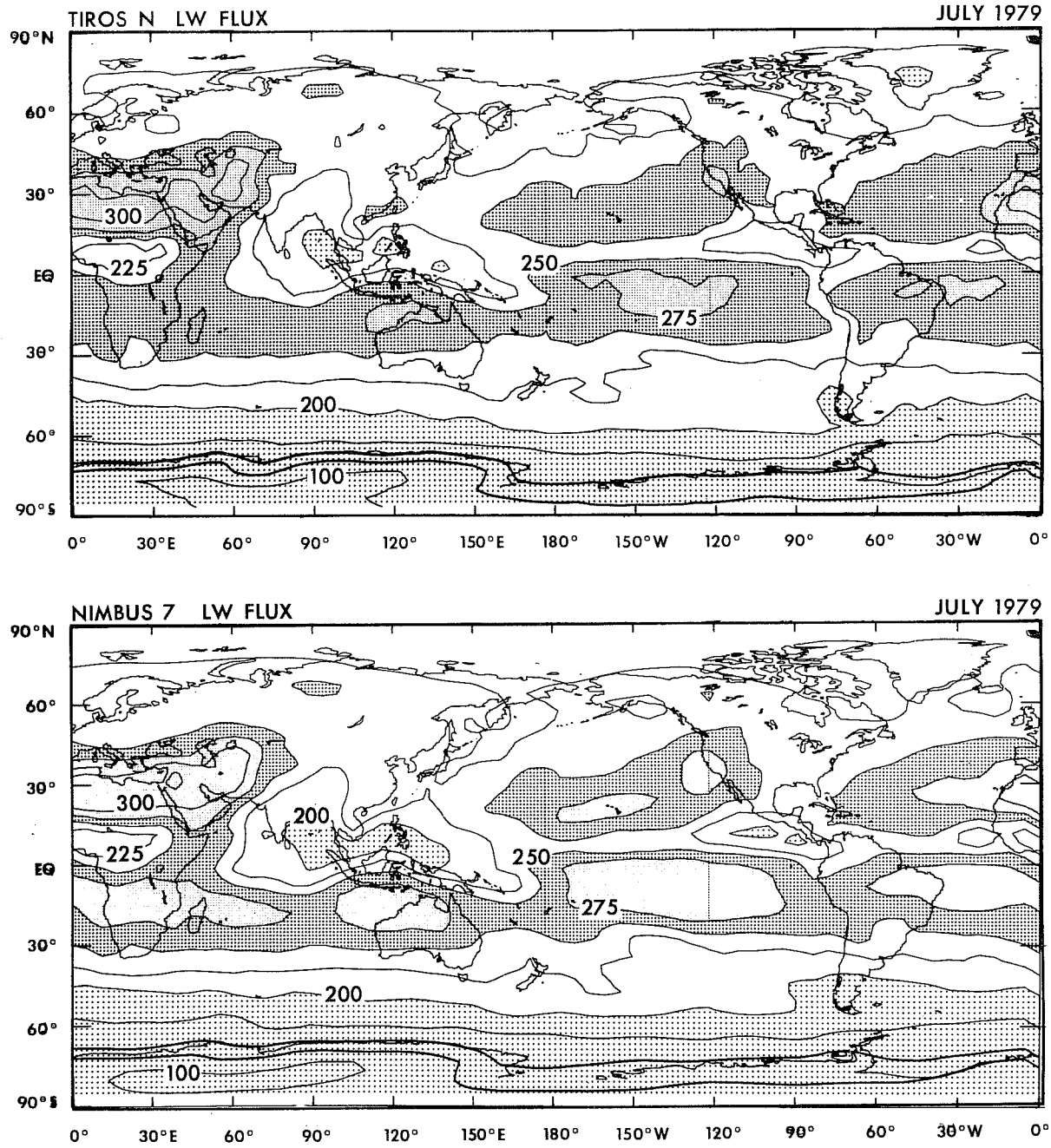

Fig. 6. Same as Fig. 5, except for outgoing longwave radiative flux.

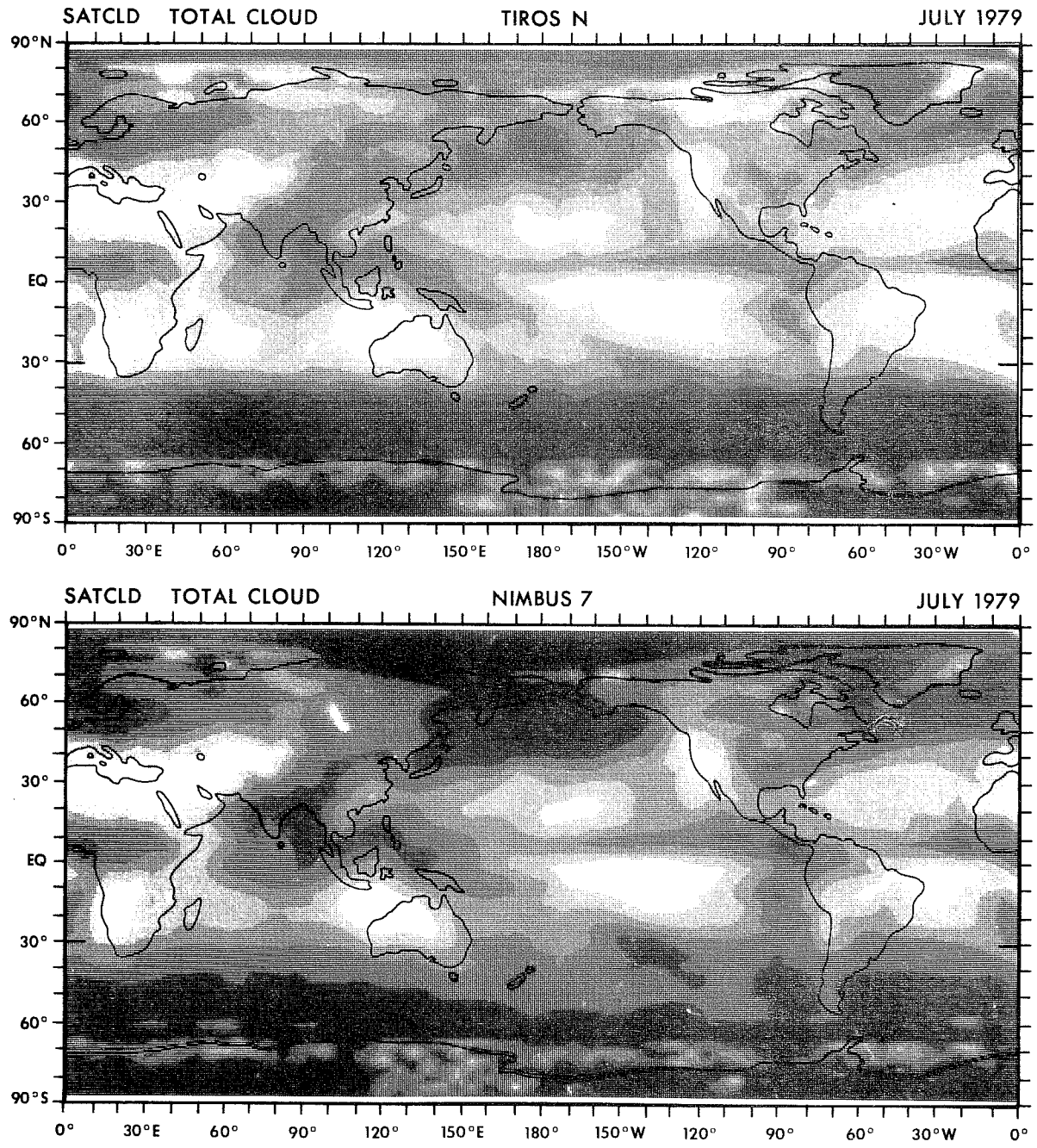

Fig. 7. July 1979 monthly mean SATCLD total cloud amount, N_T, computed from TIROS N flux (top) and NIMBUS 7 flux (bottom). 5 shades of stippling ranging from white for $N_T \leq 0.2$ to darkest for $N_T \geq 0.8$. No contours.

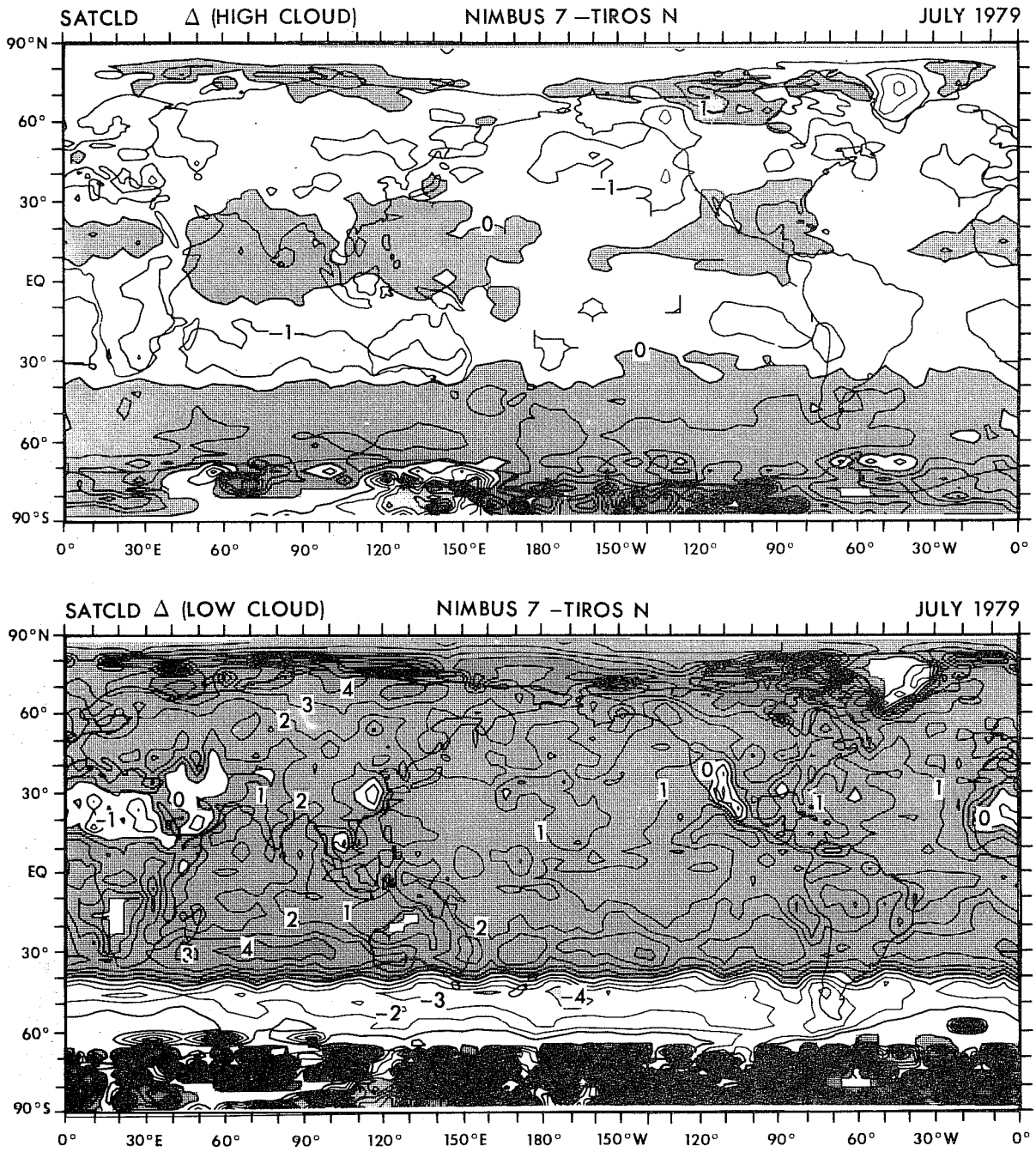

Fig. 8. July 1979 monthly mean NIMBUS 7 - TIROS N differential cloud amount. Δn_h (top), Δn_l (bottom). Contour interval = 0.1.

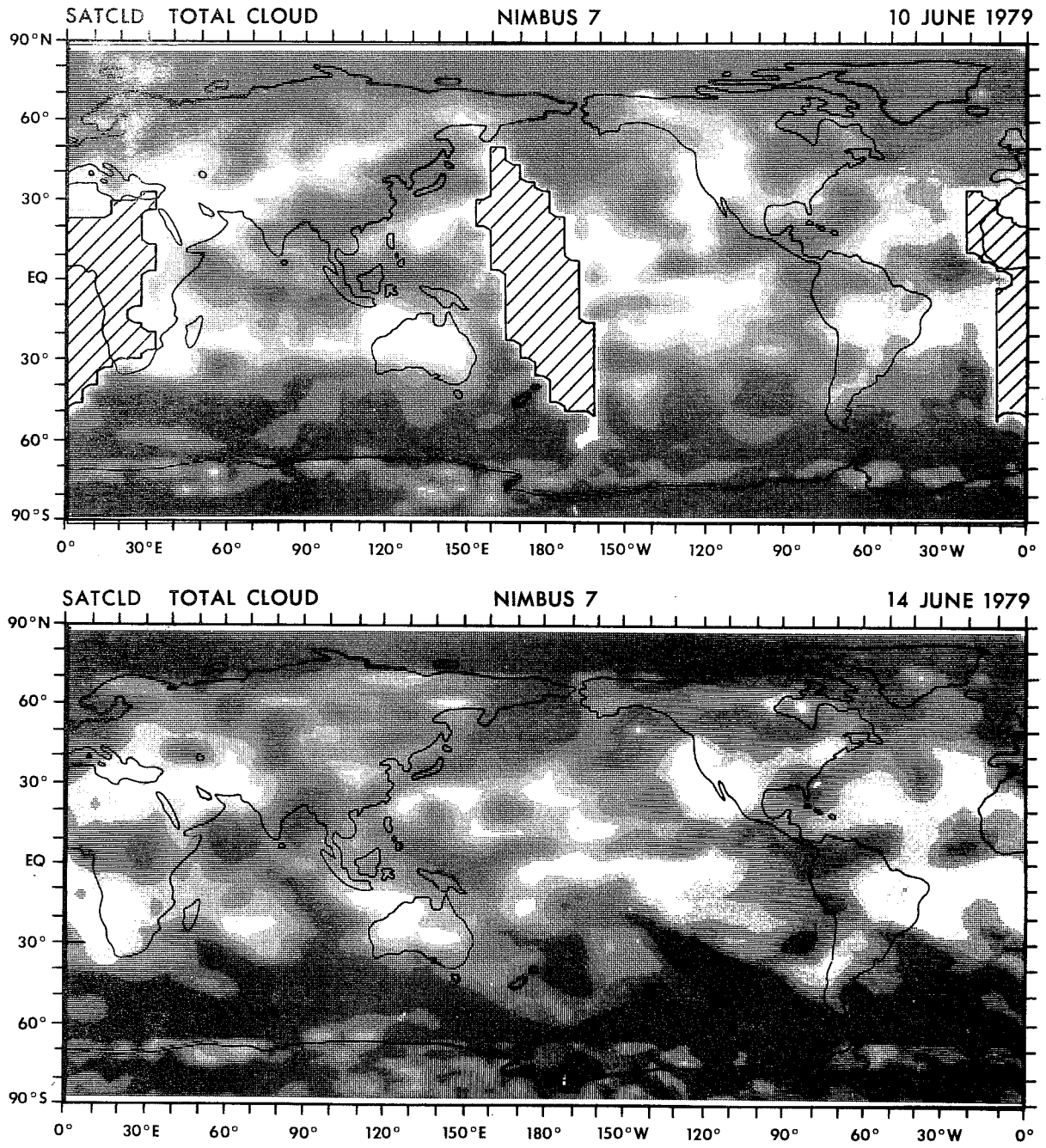

Fig. 9. SATCLD total cloud amount, N_T, computed from NIMBUS 7 flux for 10 June 1979 (top) and 14 June 1979 (bottom). 5 shades of stippling ranging from white for $N_T \leq 0.2$ to darkest for $N_T \geq 0.8$. No contours. No data in hatched region.

wave flux fields are plotted in Figure 5. Although they exhibit qualitatively similar patterns, TIROS N decreases more rapidly than NIMBUS 7 in the middle and subpolar latitudes of the southern hemisphere. Also, the TIROS N flux is less intense than NIMBUS 7 over North Africa. Meanwhile, in most other regions, the TIROS N flux tends to exceed NIMBUS 7 by 10-20 W m^{-2} except by up to 50 w m^{-2} in the arctic. The July 1979 monthly mean TIROS N and NIMBUS 7 longwave fluxes (Figure 6) are in relatively closer agreement. Even so, the NIMBUS 7 maxima and minima at tropical latitudes are perhaps 5-10 W m^{-2} more extreme than the corresponding TIROS N features.

The NIMBUS 7 analyses of daily mean shortwave flux may be more accurate, overall, than the TIROS N. Perhaps most significantly, zenith angle-dependent anisotropic correction factors (Taylor and Stowe; 1984), which account for bi-directional effects, were applied only to the NIMBUS 7 data. The corrections can be quite large at high latitudes. Of lesser importance, the NIMBUS 7 longwave and shortwave sensors are both truly broad band whereas the corresponding TIROS N sensors are narrower band. Of course, legitimate discrepancies between the two data sets could arise because of diurnal variability, as the equatorial crossing times of TIROS N and NIMBUS 7 are 1500 GMT vs. 1200 GMT local time, respectively.

Cloud intercomparisons have been made for July 1979 monthly mean conditions as well as for daily mean conditions on 10 June, 12 June and 14 June 1979. The gross structure of the July 1979 monthly mean NIMBUS 7 and TIROS N total (Figure 7), and low and especially high (not shown) effective cloud amount fields agree quite well. (Here, the total cloud amount, N_T is computed from randomly overlapping low and

high clouds, i.e., $N_T = n_1 + (1 - n_1)n_h$). Certainly, in July 1979, the NIMBUS 7 and TIROS N n_1 and N_T fields bear closer resemblance, overall, to each other, than either does to the 3DNEPH, not to mention SFCOBS or the zonal mean cloud climatology based upon Telegadas and London (1954).

Nonetheless, significant discrepancies remain. In particular, the NIMBUS 7 - TIROS N differential low cloud amount, Δn_1, (Figure 8) is substantially greater than zero in the Arctic and -0.2 to -0.3 in the southern hemisphere mid-latitude belt. Intuitively, in both regions, the NIMBUS 7 results seem more reasonable. Over much of the northern hemisphere, including the ITCZ and over the north-central Pacific, Δn_1 is systematically +.05 to .10, although $\Delta n_1 < 0$ in the vicinity of North Africa. The corresponding difference field Δn_h (Figure 8) for high cloud amount is comparatively weaker and less systematic than Δn_1, although the NIMBUS 7 extrema in the tropics may exceed the corresponding TIROS N extrema by .05 to .10. As expected, the Δn_1 and Δn_h difference fields are strongly correlated with the absorbed shortwave (ΔS) and outgoing longwave (ΔF) flux difference fields, respectively.

The period 10 June - 14 June 1979 coincides with the onset of the summer Indian monsoon. The time evolution of the daily mean total cloud amount N_T, based upon NIMBUS 7 satellite-derived radiative fluxes is illustrated in Figure 9. Again, the corresponding TIROS N results are qualitatively similar, with the same caveats as in the July 1979 monthly mean case. A prominent characteristic in both analyses is the rapid development of cloudiness over the Arabian Sea between 10 June and 14 June 1979. The streamlines at 850 mb (not shown) confirm the develop-

ment of a southwesterly circulation off the east coast of Africa and strong convergence in the monsoon region. Another characteristic is that the cloud amount fields exhibit a large transient component in many regions.

6. CRITICAL RELATIVE HUMIDITY CLOUD PREDICTION SCHEME

In most respects, this scheme resembles other critical relative humidity schemes. However, the choice of critical relative humidity is locally constrained by the observed shortwave and longwave radiative fluxes. Let n = cloud amount, h = relative humidity, h_c = central critical relative humidity and h_{con} = condensation criterion for moist convective adjustment. The variables n and h vary with longitude λ_i, latitude θ_j, vertical level σ_k and time t_m, whereas h_c depends only on λ_i and θ_j (in the simplest version) and h_{con} is constant. The predicted cloud amount $n(\lambda_i, \theta_j, \sigma_k, t_m)$ varies linearly with h over a range of relative humidities, i.e.,

$$n = \begin{cases} 0, & h < h_* \\ (\frac{1}{2})\,(1 + (h - h_c)/(h_{con} - h_c)), & h_* \leq h \leq h_{con} \\ 1 & h > h_{con} \end{cases} \qquad (5)$$

where $h_* = h_c - (h_{con} - h_c)$. By definition, n = 1/2 if $h = h_c$. Clouds are not permitted to form at the lowest GCM level, i.e., σ_9. As discussed later, h_c is determined with the aid of local longwave and shortwave radiative constraints. Assuming that $h_c(\lambda_i, \theta_j)$ is known, the time mean vertical distributions of cloud amount and associated heights of tops and bases are calculated at each horizontal grid point. The 1/2 day time averaged vertical distribution of cloud amount is assigned to up to 3 of the following categories: thin high (H), thick high (HH), thick middle-high (MH), thick low-middle (LM), thin middle (M), thick

middle (MM), thick low-middle-high (LH), and thick or thin low (L) clouds, where thick clouds straddle two or more sigma levels. Only mutually exclusive categories are permitted. For example, L, LM, and H is a permissible combination, whereas M and LH is not. Corresponding time mean heights of tops and bases are calculated as well. So are time mean cloud albedos and absorptivities, from prescribed values for H, M and L categories. (The prescribed values for thick clouds are the same as for category L).

The optimal h_c field is determined a priori by trial and error. First, the GCM is integrated 1/2 day (the present interval between radiation time steps) for 11 different values of h_c, i.e. 0.50, 0.55, 0.60, ...,1.00. Second, the corresponding sets of time averaged predicted clouds are specified to compute model-diagnosed radiative fluxes. The flux residuals ε_S and ε_F of Eqs. (1) and (2) are computed to determine a preliminary field of optimal h_c to the nearest 5%. A second iteration is performed to obtain h_c to within 0.5%. Note that the radiative constraints are much weaker here than in the original SATCLD scheme, because many more cloud parameters are varying simultaneously with h_c. Moreover, h_c does not vary with σ. Consequently, our solution may contain locally large residuals $\varepsilon_S^2 + \varepsilon_F^2$. These residuals were reduced somewhat by perturbing h_c and applying the equations

$$S_{OBS} = S_o + \left(\frac{\partial S}{\partial h_{ch}}\right)_o \Delta h_{ch} + \left(\frac{\partial S}{\partial h_{cl}}\right)_o \Delta h_{cl} + \varepsilon_S \qquad (6)$$

$$F_{OBS} = F_o + \left(\frac{\partial F}{\partial h_{ch}}\right)_o \Delta h_{ch} + \left(\frac{\partial F}{\partial h_{cl}}\right)_o \Delta h_{cl} + \varepsilon_F \qquad (7)$$

Above, h_{ch} denotes $h_c(\sigma_3)$ and h_{cl} denotes $h_c(\sigma_8)$. At intermediate σ levels, h_c is assumed to vary linearly with σ since only two observed

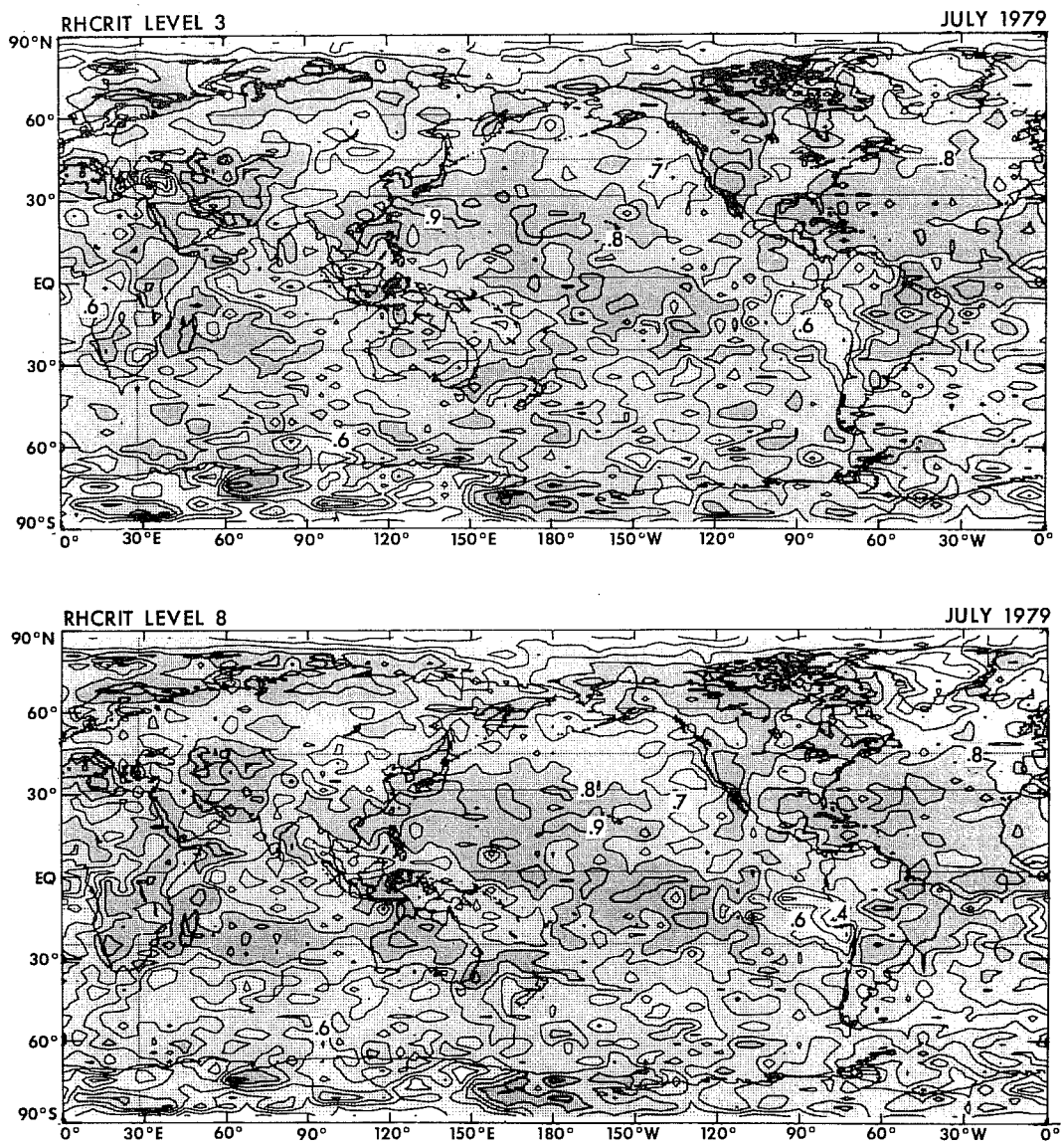

Fig. 10. Central critical relative humidity h_c at sigma level 3 (top) panel) and sigma level 8 (bottom panel), time-averaged from eight realizations. Contour interval = 0.1. Stippling: fine ($h_c \geq 0.8$), medium ($0.6 \leq h_c \leq 0.8$), and coarse ($0.4 \leq h_c \leq 0.6$).

radiative parameters are available. The perturbed values of h_{cl} and h_{ch} are $h_c - \Delta$, h_c and $h_c + \Delta$, where $\Delta = (h_{con} - h_c)/2$. Also, S_o and F_o correspond to clouds predicted for $h_{cl} = h_{ch} = h_c$. Eqs. (6) and (7) are analogous to Eqs. (1) and (2), except that the derivatives measure the sensitivity of radiative fluxes with respect to h_{ch} and h_{cl} instead of n_l and n_h, and the second order terms are discarded. These equations are convenient because explicit functional relationships between cloud top height, cloud base height, cloud albedo, cloud absorptivity and cloud amount vs. h_c are not needed to evaluate them.

The procedure just described was applied to eight quasi-independent sets of initial conditions generated by the GFDL FGGE 4-dimensional analyses for 2 July, 6 July, 9 July, 13 July, 15 July, 21 July, 25 July and 30 July 1979, 1200 GMT and the NESDIS analysis of TIROS N satellite data. The calculations required a non-trivial amount of computer time. The time means of the resulting h_{ch} and h_{cl} fields (Figure 10) were then obtained. The horizontal distributions of h_{ch} and h_{cl} are noisy, but quite similar, overall. One region where h_c varies with σ is off the Peruvian coast, where $h_{cl} < h_{ch}$ favors the production of stratocumulus. Another interesting feature is that the h_{ch} and h_{cl} fields are positively correlated with the absorbed shortwave radiative flux (cf. Figures 10 and 5).

After applying corrections to compensate for model climate drift, the scheme will be applied to a 30 day GCM integration. Analogous integrations with specified clouds are in progress. The predicted 5 day mean atmospheric circulation exhibits considerable sensitivity to the London zonal mean cloud amount climatology vs. monthly mean NIMBUS 7 SATCLD effective clouds after 10 days or so.

Also, we plan to search for universal relationships between the critical relative humidity fields (which serve as surrogate cloud amount fields) or the radiative fluxes themselves vs. various observed or model-diagnosed (grid scale) thermodynamic and dynamic variables.

7. CONCLUDING REMARKS

As an alternative to specifying fixed, externally-produced cloud amount fields in their GCMs, modellers may generate their own GCM-dependent effective cloud amount fields using an algorithm called "SATCLD". The latter has a simple formulation, is economical to apply, and employs compact, accessible analyses of satellite-derived radiative fluxes. SATCLD low and high cloud amounts are constrained to be consistent, locally, with observed long- and shortwave radiative fluxes. Radiative consistency in the modeller's GCM is facilitated by the use of its own cloud-radiation model and surface albedo field to generate the clouds. Weaker radiative constraints may be incorporated into a fully interactive cloud prediction scheme.

SATCLD effective cloud amount fields seem plausible, in many respects, despite some unrealistic features. Moreover, some of the latter respond favorably to an improved specification of surface albedo and/or analysis of satellite-derived radiative flux data. In principle, more realistic radiatively constrained clouds could be generated by: (1) obtaining more representative estimates of observed, daily mean radiative fluxes and their diurnal variation from geostationary satellites or from an expanded polar orbiting satellite network; (2) incorporating state of the art cloud-radiative parameterizations into GCM's to reduce their radiative bias; (3) incorporating additional cloud properties into the SATCLD scheme such as middle cloud amount, heights

of cloud tops, cloud type, or cloud liquid water content, thereby obtaining more realistic model-diagnosed vertical profiles of net radiative cooling. If the augmented SATCLD scheme is to remain deterministic, each additional cloud property should be matched by an additional radiative constraint. Possible candidates include in situ measurements of tropospheric radiative flux divergence, radiative flux measurements at the surface, and/or narrow band radiances from 2 or 3 informative spectral channels.

8. REFERENCES

Fels, S.B. and M.D. Schwarzkopf, 1975: The simplified exchange approximation: A new method for radiative transfer calculations. J. Atmos. Sci., 32, 1476-1488.

Gordon, C.T., 1983: A scheme for generating radiatively consistent, effective clouds at two atmospheric levels. Fifth Conference on Atmospheric Radiation held 31 October - 4 November 1983, Baltimore, MD, 280-283.

Gordon, C.T. and W.F. Stern, 1982: A description of the GFDL global spectral model. Mon. Wea. Rev., 110, 625-644.

Gordon, C.T., R. Hovanec and W.F. Stern, 1984: Analyses of monthly mean cloudiness and their effect on GCM-diagnosed radiative fluxes. J. Geophys. Res., 89, D3, 4713-4738.

Gruber, A., 1978: Determination of the earth-atmosphere radiation budget from NOAA satellite data. NOAA Technical Report, NESS 76, National Environment Satellite Service, WWB, Washington, D.C. 20233.

NASA, 1978: The NIMBUS 7 Users' Guide. Prepared by The Landsat/Nimbus Project, Goddard Space Flight Center, NASA, Charles R. Madrid, ed.

Payne, R.E., 1972: Albedo of the sea surface. J. Atmos. Sci., 29, 959-970.

Ploshay, J.J., R.K. White, and K. Miyakoda, 1983: FGGE level III-B daily global analyses, Part 1, NOAA Data Rep. ERL GFDL-1, Geophys. Fluid Dyn. Lab., Princeton, N.J.

Posey, M.W. and P.F. Clapp, 1964: Global distributions of normal surface albedo. Geofiscia International, Mexico City, D.F., Mexico, 4, No. 1, 33-48.

Ramanathan, V.E., E.J. Pitcher, R.C. Malone and M.L. Blackmon, 1983: The response of a spectral general circlation model to refinements in radiative processes. J. Atmos. Sci., 40, 605-630.

Robock, A., 1980: The seasonal cycle of snow cover, sea ice and surface albedo, Mon. Wea. Rev., 108, 267-285.

Schneider, S.H., 1972: Cloudiness as a global climatic feedback mechanism: The effects on the radiation balance and surface temperature variations in cloudiness. J. Atmos. Sci., 29, 1413-1422.

Stephens, G.L., and P.J. Webster, 1981: Clouds and climate: Sensitivity of simple systems. J. Atmos. Sci., 38, 235-247.

Taylor, V. R. and L. L. Stowe, 1984: Reflectance characteristics of uniform earth and cloud surfaces. J. Geophys. Res., 89, No. D4, 4987-4996.

Telegadas, K. and J. London, 1954: A physical model of the northern hemisphere troposphere for winter and summer. Sci. Rept. No. 1, contract AF 19(122)-165, Research Division, College of Engineering, New York University, 55 pp. [DOC AD 032472].